A novel biogenic synthesis of Ag@biochar nanocomposite for wastewater treatment

Journal:	*ACS Omega*
Manuscript ID	ao-2021-06286x
Manuscript Type:	Article
Date Submitted by the Author:	08-Nov-2021
Complete List of Authors:	Eltaweil, Abdelazeem; Alexandria University Faculty of Science, Chemistry Abdelfatah, Ahmed; Alexandria University Faculty of Science, Environmental Science Hosny, Mohamed; Alexandria University Faculty of Science, Department of Environmental Sciences Fawzy, Manal; Faculty of Science, Environmental Sciences

A novel biogenic synthesis of Ag@biochar nanocomposite for wastewater treatment

Abdelazeem S. Eltaweil , Ahmed M. Abdelfatah , Mohamed Hosny* and Manal Fawzy

Abstract

A facile, eco-friendly, cost-effective, novel, and sustainable route for the synthesis of silver-loaded biochar nanocomposite (Ag@biochar) using *Chenopodium amperosidies* L. extract and biomass is reported for the first time in this study. UV analysis appeared at 420 nm indicating the formation of silver nanoparticles. The bandgap energy of Ag@biochar was 1.9 eV confirmed its potential use as a photocatalyst. XRD analysis indicated the crystal structure of the green synthesized Ag@biochar while FT-IR, EDX, and XPS analyses ensured the successful bioformation of the composite. AgNPs on the surface of biochar were predominantly spherical with a size range of 25-35 nm. A zeta potential of -5.87 mV designated the stability of Ag@biochar. Testing the photocatalytic potential of this novel nanocomposite to remove MB from wastewater demonstrated its remarkable efficiency. Ag@biochar was also shown to be a powerful broad-spectrum antimicrobial agent against both gram-positive and negative bacterial species as well as *Candida albicans*.

Synopsis: A novel, cost-eefective, and environmentally-safe Ag@biochar nanocomposite was used as a photocatalyst for wastewater treatment and disinfection.

Keywords: Green; Silver; Biochar; Antibacterial; Photocatalysis

1. Introduction

There is no doubt that water is an essential resource for sustaining all forms of life, and its treatment, particularly in the industrial sectors, is a necessity to eliminate the environmental and health risk [1-2]. Due to the technological development and the dramatic increase in industrial activities, the environment became seriously deteriorated especially aquatic ones [3]. Toxic organic pollutants are important environmental hazards that seriously threatened both aquatic and terrestrial ecosystems [4-5]. Among these organic pollutants, dyes from the textiles industry are hazardous effluents containing toxic complex components that without appropriate treatment severely impact the environment and exerting harmful health effects including difficulties in breathing, vomiting, eye burns [6]. Therefore, how to effectively remediate organic pollution of the environment has become more and more challenging [7-8].

In recent years, biochar has gradually entered people's vision. Biochar is a carbon-rich solid, which is obtained by heating biomass in an oxygen-depleted environment, such as wood, manure with little or no oxygen. As a kind of adsorbent, biochar, with a porous structure similar to activated carbon, is the most commonly used and effective adsorbent in the world to remove various pollutants in water. However, among the limitations of using biochar for wastewater treatment are the relatively low surface area and the influence of abiotic and/or biotic processes which can diminish its effectiveness in certain applications.

Despite several scientific pieces of research on the biochar applications, recent researches have been focused primarily on the modification of the biochar using nanomaterials and other structures to improve its performance in environmental applications and remediation potentials.

In the present study, biochar derived from *Chenopodium amperosidies* L. (*C. amperosidies*) biomass was amended by impregnating it with green synthesized AgNPs using the shoot extract of the same species. As compared to conventional synthesis, green synthesis seeks to avoid secondary impacts, by either (i) using sustainable materials, or (ii) consuming less energy in the synthesis process, aspiring for ambient synthesis reaction conditions. Plant extracts and phytochemicals such as flavonoids, terpenoids, and phenolic compounds had been proved to be efficient reducing and stabilizing agents for the synthesis of metal and metal oxide nanoparticles in a facile and single-step process. Therefore, biosynthetic approaches, specifically those using plant extracts, arose as a faster, cheaper, environmentally safer, and more efficient route to synthesize nanomaterials.

Among metal nanoparticles, AgNPs are predominantly utilized in a variety of medicinal and environmental applications such as diagnosis, cancer treatment, gene, and drug delivery and degradation of toxic organic pollutants because of their oxidation resistance, biocompatibility, stability, and optical properties [9]. Consequently, AgNPs were selected to be green synthesized by the aqueous extract of *C. amperosidies* and further impregnated on the same plant biochar. The use of plant extracts for the green synthesis of Ag@biochar nanocomposite, however, remains an underexplored research topic till now.

As a result of the growing problem of multidrug-resistant bacteria, on which conventional antibiotics have little or no effect, AgNPs have aroused as a proper and alternative antibiotic agent that was proved to be highly efficient particularly AgNPs that are green synthesized. The antibacterial action of AgNPs has been improved on a nanoscale with the emergence of nanotechnology, and currently, it is utilized to manage a variety of human and animal diseases. The material size, capping agent of AgNPs, the content, and phytochemical structure are considered to be critical factors in determining their antimicrobial efficacy.

Herein, we aimed to fabricate Ag@biochar nanocomposite via a novel and complete green route in which the *C. amperosidies* acts as a green source of biochar support and its extract acts as a reducing agent for silver ions avoiding the use of chemicals in the whole process. Therefore, *C. amperosidies* role is twofold, firstly the production of biochar from readily available biomass and secondly the reduction of Ag^+ ions. The photocatalytic potentiality of the fabricated Ag@biochar nanocomposite was evaluated in the removal of MB from polluted water. Furthermore, the Ag@biochar nanocomposite was examined as an antibacterial and antifungal agent.

2. Results and discussion

2.1. Characterization of Ag@biochar

2.1.1. UV-Visible spectroscopy

Generally, UV-Visible spectroscopy is deemed to be a very basic and efficient tool that is utilized to indicate the successful reduction of metal salts into nanoparticles such as gold, silver, and platinum. The surface plasmon resonance peak of Ag@biochar was quite obvious (**Fig. S1a)** at the wavelength of 420 nm which is in line with lots of other previous studies that targeted the green synthesis of AgNPs utilizing extracts of numerous plant species [10]. Regarding the UV-Vis spectrum of pristine biochar, there were no peaks observed at all (**Fig. S1b**). Furthermore, it has been noticed that the bandgap energy (Eg) of Ag@biochar was elucidated by the Tauc plot as shown in **Fig. S1c.** The Kubelka-Munk function $(\alpha hv)^2$ was plotted against band gap energy (E_g = hv = $hc\ \lambda$), where α is absorption coefficient, h is the Plank's constant, and v is the frequency of radiation. The bandgap is then estimated by extrapolating the linear portion of the graph to y-axis zero value and it was about 1.9 eV (**Fig. S1c**) which is better than the bandgap of other biochar composites such as TiO_2@biochar [11], TiO_2–BSP [12] GQD–TiO_2 and N-biochar composites which had a bandgap ranging between 3.30 and 2.28 eV [13]. Thus, the deposition of AgNPs on the surface of biochar decreases the bandgap energy of the pristine biochar as demonstrated in **Fig. S1d**. This also supports the creation of new energy states in Ag@biochar nanocomposite samples caused by Ag-C bonds formed as a result of AgNPs association with biochar's carbon content. Therefore, Ag@biochar could be harnessed in the photocatalytic degradation of MB.

2.1.2. XRD analysis

XRD spectrum of the pristine biochar (**Fig. S2a**) exhibited characteristic peaks at 28.5°, 40.6° and 50.26° which were indexed to (002), (100) and (004) planes, respectively, as previously mentioned by other workers [14], whereas the XRD pattern of Ag@biochar composite (**Fig. S2b**) demonstrated the same peaks of the pristine biochar yet with a lower intensity and other new peaks at 32.1°, 46.06° and 62.5° which are indexed as (111), (200) and (220) planes referring to face-centered-cubic (FCC) silver [JCPDS file number 04-0783] . Moreover, the (111) plane, in accordance with many workers [15], was the preferred growth direction for the phytosynthesized Ag@biochar nanocomposite. These findings confirmed the successful reduction of silver ions on the surface of the biochar producing Ag@biochar nanocomposite.

2.1.3. FT-IR analysis

FT-IR spectral analysis shown in **Fig. S2c** was carried out to investigate the surface modification of biochar with AgNPs. Some oxygen-containing groups were detected on the surface of the pristine biochar such as the hydroxyl group (OH). A spectral band for the O-H stretching vibration was found at 3274 cm^{-1} that shifted to lower wavenumber (a lower intensity) at 3308 cm^{-1} in the IR spectrum of Ag@biochar indicating the role of *C. amperosidies* phytoconstituents containing OH functional group such as flavonoids, tannins, and alkaloids [16] in being oxidized and resulting in the reduction of silver ions into AgNPs on the surface of the biochar. The peaks near 1600 cm^{-1} in both samples were assigned to aromatic C=O ring stretching which is also attributed to the same phytoconstituents [17]. Also, peaks near 1430 cm^{-1}, likely due to the aromatic C-O ring stretching, In addition, other aromatic stretching peaks between 1000 and 1200 cm^{-1} are suggested to be resulting from the incomplete pyrolyzed *C. amperosidies* feedstocks such as cellulose and hemicellulose as mentioned in previous biochar research articles [17].

2.1.4. SEM and EDX analysis

The SEM technique was used to identify morphological surfaces features of pristine biochar and biochar after modification with AgNPs and to provide information on porosity and surface structure of both materials, size, and shape of AgNPs that are dispersed on the biochar surface as it was previously utilized by many workers [18]. The pristine biochar and Ag@biochar composite were illustrated in **Fig. 1a, b** and **Fig. 1c, d** in a respective manner. In this study, SEM images revealed a porous structure in both biochar samples. Porosity is commonly considered as a consequence of the release of matter in the form of small volatile molecules including CO, CO_2, CH_4, and H_2O during the thermal conversion process. The ubiquitous distribution of AgNPs on the surface of biochar is quite obvious in **Fig. 1c, d** as AgNPs appeared as white particles dispersed on the biochar's surface which was not found in pristine biochar sample (**Fig. 1a, b)**. Thus, confirming the successful green synthesis of Ag@biochar nanocomposite. The appearance of strong signals for elemental Ag at 3 and 3.3 keV in the current study as shown in **Fig. 1e** was similar to previous results that were reported by other workers [19]. Thus, confirming the green synthesis of Ag@biochar nanocomposite. The Elemental analysis of the Ag@biochar's surface (**Fig. 1e**) indicated that the total zero-valent Ag percentage in the sample was 1.89% which is quite close to the percentage of silver ions that was initially dispersed on the surface of the biochar which was 2% silver ensuring the great efficacy of the aqueous extract of *C. amperosidies* in the reduction of silver ions into AgNPs on the biochar's surface. Furthermore, it has to be mentioned that the particle size of the dispersed AgNPs on the surface of the biochar in the current investigation was in the range of 25 to 35 nm.

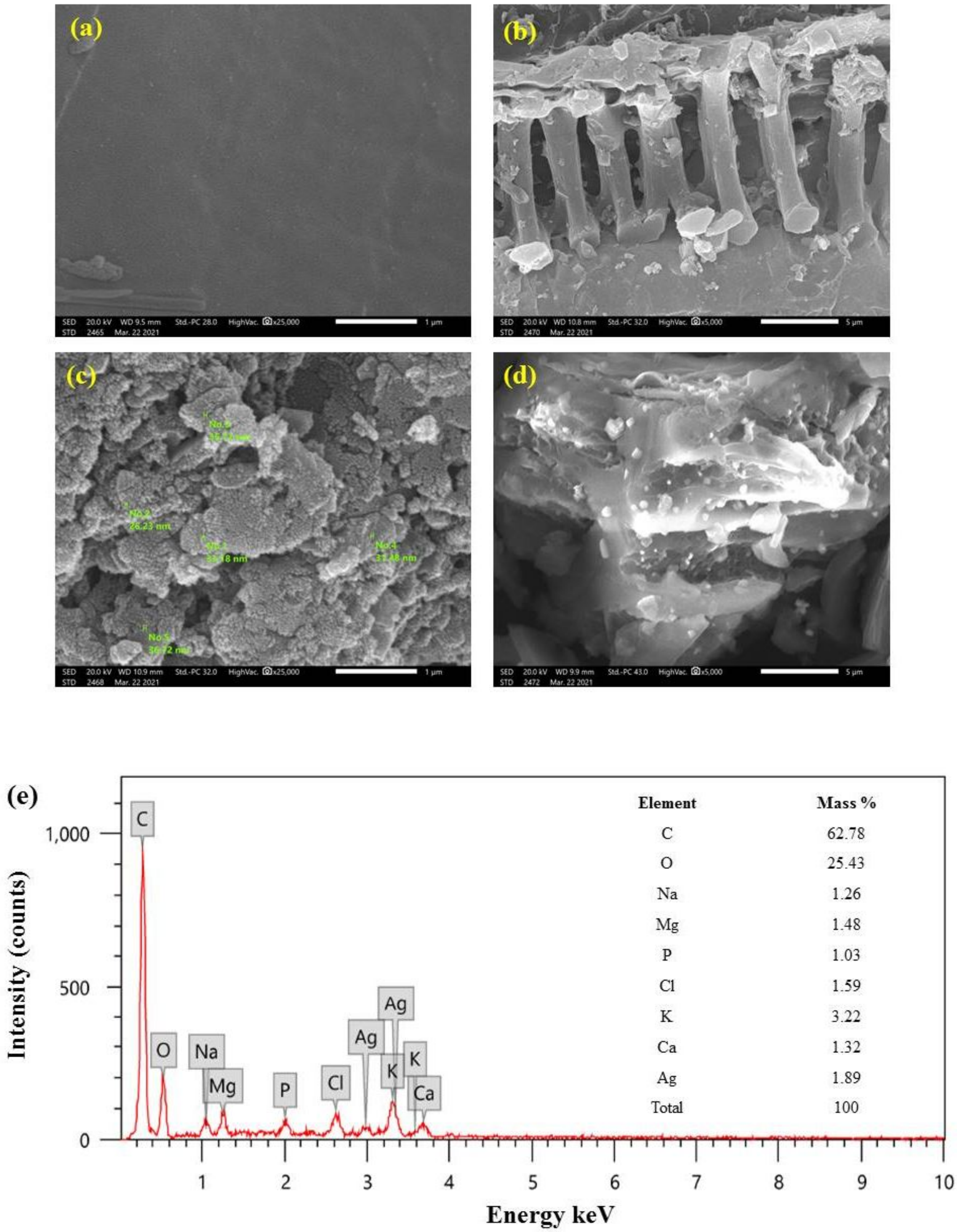

Fig. 1. SEM photomicrograph of **(a, b)** Ag@biochar, **(c, d)** biochar, and **(e)** EDX analysis.

2.1.5. XPS analysis

A further investigation was carried out using XPS, a powerful surface-sensitive analytical tool, to analyze the chemical compositions, ionic characteristics, and bonding configuration differences between biochar and Ag@biochar. Two major surveys for biochar and Ag@biochar indicating the presence of C1s, O1s, N1s, and Na1s as major constituents in addition to Ag3d in the case of Ag@biochar nanocomposite as presented in **Fig. 2a** and **b**, respectively. **Fig. 2c** shows C1s spectrum of the biochar and the different peaks at 284.63 eV, 286.12 eV, and 288.21 eV are attributed to C–C, C=C, C–O and O–C–O, respectively, which is mainly derived from the polyphenol's groups in the plant. In comparison with the C1s of the Ag@biochar (**Fig. 2f**), there is a noticeable shift in the C-O peak at 288.21 eV to 286.26 eV indicating the reduction of Ag ions into silver nanoparticles on the surface of the biochar. The binding energies of the O1s spectrum of the biochar (**Fig. 2d**) show that the binding energy peak at 531.05 eV, 532.45, eV and 535.02 eV were attributed to the O atoms from sulphonate function [20], S=O group [21] and C-O group [22], respectively. The O1s of the Ag@biochar (**Fig. 2g**) shows that there was also an obvious shift in the C-O at 535.02 eV to 532.84 eV denoting the bounding of AgNPs to the surface of biochar. In addition, the N1s spectrum of biochar demonstrated the appearance of C-N at 399.66 eV as shown in **Fig. 2e** that shifted to 399.88 eV in the case of Ag@biochar (**Fig. 2h)** indicating the formation of AgNPs and its probable interaction with nitrogen [23]. The deconvoluted peaks of the Ag3d spectrum (**Fig. 2i**) show the peak binding energies at 366.4 eV, 368.1 eV, and 372.5 eV. Among these, the peak at 368.1 eV corresponded to silver oxide (Ag–O) and the peaks at 366.4 eV and 372.5 eV corresponded to the unbound Ag $3d_{5/2}$ and Ag $3d_{3/2}$, respectively of metallic silver nanoparticles as the binding energy splitting value was almost 6 eV similarly to [24]. The current XPS analysis confirmed the presence of AgNPs and Ag-O indicating the successful distribution of silver on the surface of the biochar and also the successful reduction of Ag ions into AgNPs on the surface of the biochar.

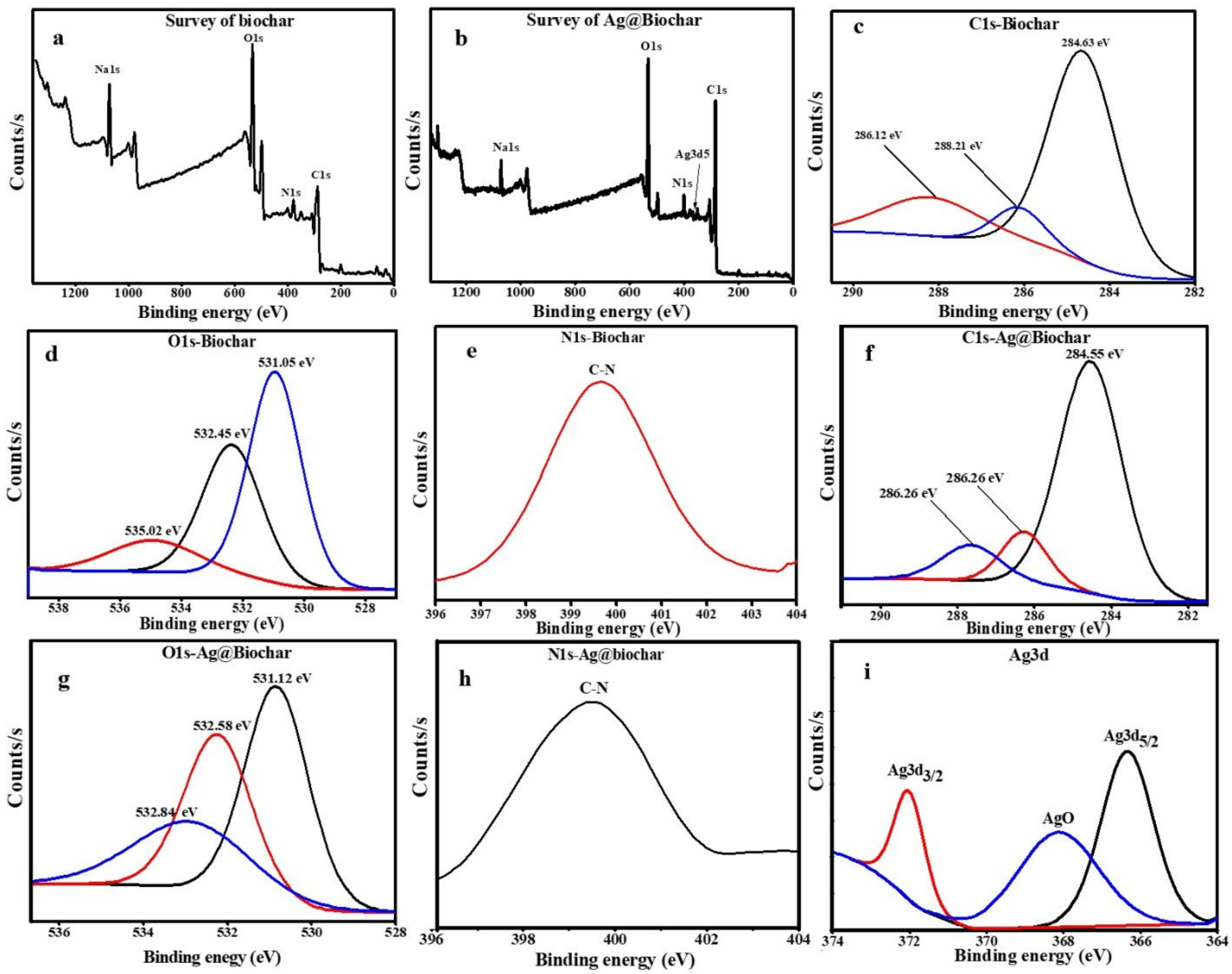

Fig. 2. XPS spectra for biochar survey **(a)**, Ag-biochar survey **(b)** biochar C1s **(c)**, O1s **(d)**, N1s **(e)**, Ag-biochar C1s **(f)**, O1s **(g)** N1s **(h)**, and Ag3d **(i)**.

2.1.6. Zeta potential

Zeta potential is one of the main tools that are harnessed to express the stability of nanoparticles in an aqueous solution [25]. The recorded Zeta potential for the biochar was -9.25 mV as displayed in **Fig. S3b**, while in the case of Ag@biochar composite it was recorded as -5.87 mV as shown in **Fig. S3a** that was similar to other results [26]. A probable justification for the decrease in the zeta potential value of Ag@biochar compared to the pristine biochar could be the interaction between the biochar and the deposited silver that resulted in oxidation of some of the functional groups contributing to the negative surface charge such as COOH and OH. Consequently, it was concluded that the Ag@biochar of the current work acquired stable dispersal potential in the solution and also indicating its potential use as an adsorbent and a photocatalytic material for the removal of cationic dyes such as MB.

2.1.7. Thermal gravimetric analysis

TGA analysis of biochar and Ag@biochar are represented in **Fig. 3**. The two samples exhibited a first regular step with approximate weight loss of 15% up to 150 °C which could be attributed to the loss of the moisture content [27-28]. Then the two samples were almost stable up to 360 °C. After that, there is a rapid weight loss from 360 to 800 °C for both samples which could be assigned to the decomposition of cellulosic and hemicellulosic compounds as well as lignin. However, the weight loss of Ag@biochar was less than that of the pristine biochar which could be attributed to the capability of silver nanoparticles in resisting thermal degradation.

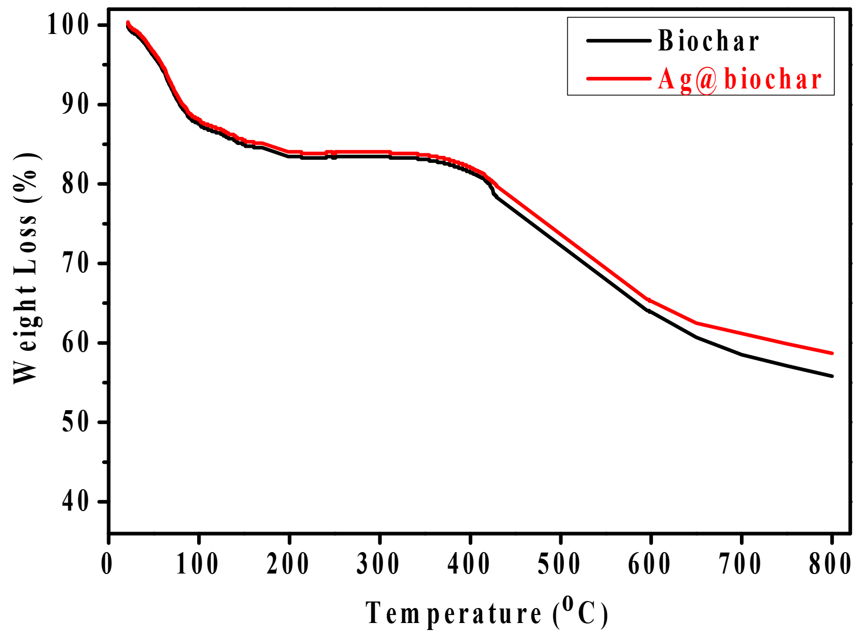

Fig. 3. TGA curves of biochar and Ag@biochar

2.1.8. BET analysis

The surface area of biochar and Ag@biochar samples were determined using the multipoint BET method based on the nitrogen adsorption-desorption isotherm, while their total pore volumes were determined using the Barette, Jovner & Halenda (BJH) process. **Fig. 4** represents the N_2 adsorption/desorption isotherms of biochar and Ag@biochar nanocomposite. It is obvious from the isotherms that both biochar and Ag@biochar exhibit type IV. The specific surface area S_{BET} of biochar and Ag@biochar were found to be 64.36 and 47.61 m^2/g, respectively. It is obvious that specific surface area of pristine biochar decreased upon the incorporation of AgNPs on its surface. In addition, the pore volume of biochar and Ag@biochar are 0.033 and 0.024 m^3/g, respectively.

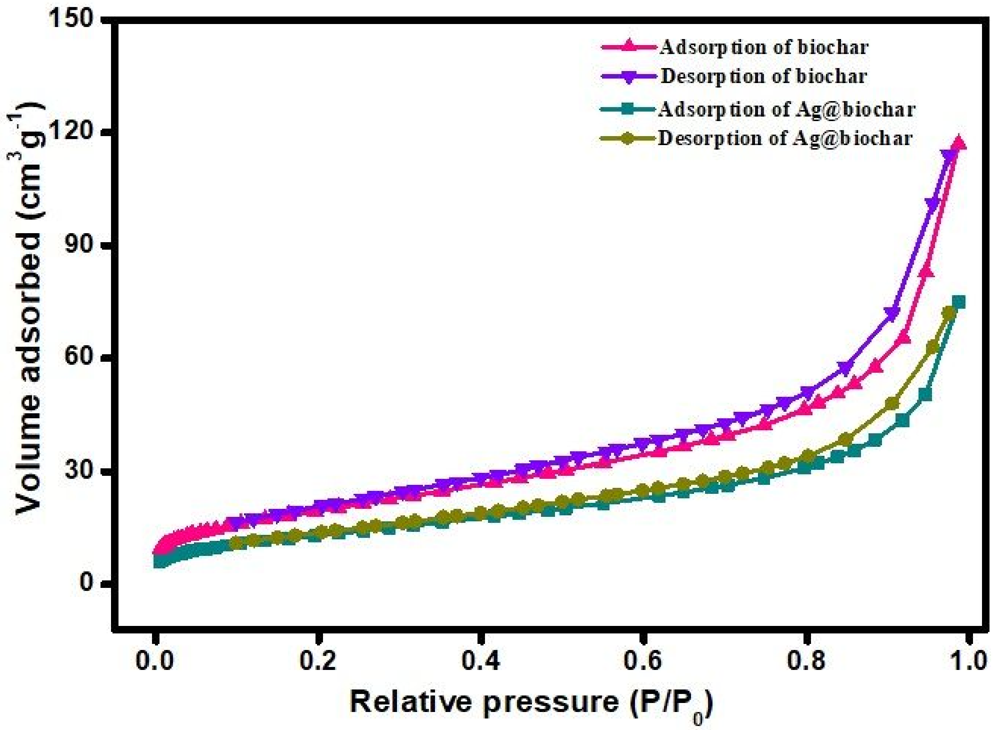

Fig. 4. N_2 adsorption/desorption isotherm of biochar and Ag@biochar.

2.2. Photocatalytic study

Photocatalytic efficiency of the green synthesized Ag@biochar nanocomposite towards the photodegradation of MB was investigated, employing a 300W xenon lamp as a visible light source ($\lambda > 420$nm), using different concentrations of MB (10-50ppm). Firstly, 5mg of Ag@biochar nanocomposite was dispersed in an aqueous solution and vigorously stirred for 30 min to attain adsorption-desorption equilibrium and to facilitate the diffusion of MB molecules to the matrix of the nanocomposite, before being exposed to visible light to initiate the photocatalytic process. Afterwards, the concentration of MB was measured during the reaction course by following the intensity of the characteristic UV-Vis absorption peak of MB at 664 nm. As a result, Ag@biochar nanocomposite exhibited an immediate and outstanding photocatalytic efficacy of 98.72% at the concentration of 10 ppm (**Fig. S4a)** and excellent photocatalytic efficiencies of 88.4%, and 84% at the concentrations of 25 ppm and 50 ppm in 75 and 210 min, respectively (**Fig. S4b, c)** which was mainly attributed to the outstanding synergy between AgNPs that enhance the visible light harvesting capability of the nanocomposite due to the SPR phenomenon, and the graphitic structure of the biochar that ameliorates the interfacial charge separation. Thus, quenching the electron-hole pairs recombination which in turn improves the generation of ROS (reactive oxygen species) that drive the photocatalytic degradation process. Consequently, it displayed superior photocatalytic performance. Remarkably, UV-vis absorption peak at 664 nm showed a slight blue shift during the reaction course that could be attributed to diminished ethyl group and benzene ring within MB structure. However, Ag@biochar nanocomposite revealed a slight decrease in the photocatalytic efficiency at elevated concentrations of 25 ppm and 50 ppm comparable to 10 ppm that may be caused by the intense color of MB that causes turbidity, and thus shields the visible light from striking the photocatalyst. The time effect on the photodegradation process of MB at concentrations of 25 ppm and 50 ppm in the presence of Ag@biochar is shown in **Fig. S5a, b.**

2.2.1. Possible adsorption and photocatalytic Mechanism for removal of MB by Ag@biochar nanocomposite

Owing to the graphitic structure and the extended functionality of the biochar, Ag@biochar nanocomposite displayed an ultra-adsorption capacity of MB in contact time 30 min. Such behavior was elucidated through the electrostatic attraction, π-π stacking, and monolayer chemisorption complexation with the carboxylate groups of the biochar. Additionally, MB could be adsorbed *via* complexation of AgNPs with the active functional groups of MB. Accordingly, this adsorption capability further boosted the photocatalytic performance of the nanocomposite. As a result, visible light Irradiation of Ag@biochar nanocomposite generates electron-hole pairs due to the SPR phenomenon of AgNPs. Thus, generating ROS such as superoxide anion and hydroxide radicals *via* reaction with oxygen and H_2O molecules adsorbed onto Ag@biochar nanocomposite which in turn initiate the photocatalytic degradation of the adsorbed MB molecules. Also, the generated h^+ in the valence band (VB) can capture an electron from the adsorbed dye molecules resulting in oxidation of MB as shown in **Fig.S6**. Furthermore, it is worth mentioning that biochar reveals dual functions comprising the ease of charge separation through the extended graphitic structure that facilitates the charge transfer, and thus restrains the charge recombination as well as the presence of persistent free radicals (PFRs) that can also generate ROS which in turn boost the photocatalytic degradation of MB as shown in the following mechanism [29].

$$Ag^{o} + h\upsilon\ (visible) \rightarrow Ag\ (h^{+} + e^{-}) \quad (1)$$

$$e^{-} + O_2 \rightarrow O_2^{\cdot -} \quad (2)$$

$$h^{+} + H_2O \rightarrow H^{+} + .OH \quad (3)$$

$$H^{+} + O_2^{\cdot -} \rightarrow HO_2^{\cdot} \quad (4)$$

$$2\ HO_2^{\cdot} \rightarrow H_2O_2 \rightarrow O_2 + .OH + OH^{-} \quad (5)$$

$$PFRs + O_2 \rightarrow O_2^{\cdot -} \quad (6)$$

$$O_2^{\cdot -} + h^{+} + \cdot OH + MB \rightarrow CO_2 + H_2O + \text{by products} \quad (7)$$

To evaluate the photodegradation capacity of the synthesized Ag@biochar, it was compared with other catalysts reported in other research works. Such a comparison was summarized in **Table 1** and confirmed that Ag@biochar exhibits a good degradation capacity compared to other catalysts and it can be considered as a promising material for the removal of toxic organic pollutants such as MB.

Table 1. Comparison between Ag@biochar and other catalysts according to their photodegradation capacity of MB.

catalyst	Photodegradation capacity (%)	Dye concentration (mg/L)	Time (min)	Ref.
AgNPs	82.8	60	180	[30]
AgNPs	92.1	25	14	[31]
Ag/ZnO	81.2	25	240	[32]
Ag/ZnO nanocomposite	94.3	10	120	[33]
Ag@biochar	88.4	25	75	This study
Ag@biochar	84.0	50	210	This study

3.3. Antimicrobial study

2.3.1. Antibacterial study

Metallic nanoparticles are deemed to be useful disinfectant agents such as silver, zinc oxide, and gold nanoparticles which are the most widely used. Silver nanoparticles' (AgNPs) well-known inhibitory actions have been employed in a variety of medicinal applications. Particularly the inhibition of positive and negative bacterial strains. Nanocomposites prepared by mixing AgNPs with other nanoparticles, biopolymers, and other materials have also been proved to have efficient antimicrobial effects. Consequently, the antimicrobial efficacy of Ag@biochar synthesized in this study was tested against different gram-negative and gram-positive bacteria such as *Escherichia coli*, *Pseudomonas aeruginosa*, and *Klebsiella pneumonia* (gram negative bacteria) and also gram positive bacteria including *Bacillus subtilis* and *Staphyllococus aureus*. The obtained results showed that the inhibition zone was 19 mm in the case of *Pseudomonas aeruginosa*, 18 mm for *Klebsiella pneumonia*, 22 mm for *Bacillus subtilis*, and no growth was detected at all in the case of *Escherichia coli* meaning that Ag@biochar was so efficient against *Escherichia coli* as it prevented the growth of the bacteria. The current findings imply that Ag@biochar may have antibacterial properties by altering the structure of the cell membrane and preventing normal budding owing to the loss of membrane integrity. Thus, obtained results (**Fig. 5**) indicated that the novel synthesized (Ag@biochar) is a promising and powerful antibacterial that could be used against gram-negative and also gram-positive bacteria with a high concentration ($2x10^8$ CFU/mL).

The specific mechanism by which nanoparticles generate antimicrobial effects is yet unknown. However, it is suggested that when nanoparticles come into direct contact with microbial cells, they result in cell death by disruption of the cell membrane, induction of hyperthermia, disturbance of nutrient uptake, and other physiological disorders.

2.3.2. Antifungal study

Candida albicans is a prevalent yeast that colonizes the skin and mucosal membranes in opportunistic fungal infections all over the world. *Candida* is an opportunistic part of the natural flora of the skin, mouth, vagina, and feces. In nature, they can be found on plant leaves, water, and dirt. *Candida albicans* is a pleomorphic mold that is found in the human and animal bodies . It is worth noting that recent reports indicated an increased rate of *Candida albicans* co-infection during the COVID-19 pandemic. With an incomplete understanding of the pathogenesis and without any causative therapy available [34]. Therefore, the search for a new material that could be used as an antifungal agent with high efficiency is supposed to be of great importance. The green synthesized Ag@biochar in this study was tested as an antifungal agent against *Candida albicans* with a high concentration ($2x10^8$ CFU/mL) and it did stop the growth of *Candida* with an inhibition zone of 16 mm (**Fig. 5**). Consequently, Ag@biochar was concluded to be an efficient and promising antifungal agent.

Regarding the antifungal mechanism, The use of Ag@biochar hindered the fungal cell wall as well as other physiological processes. Additionally, Ag@biochar can result in DNA fragmentation and nuclear condensation during different types of cell death. As well as inhibition of respiratory chain, induction of hyperthermia and disturbance of nutrient uptake. Finally, all these interactions will end up with fungal cell death (Apoptosis) as previously mentioned by many workers [35].

When a comparison was drawn among the diameter of the inhibition zone for different green-synthesized samples of AgNPs and AgNPs composites including the green synthesized composite (Ag@biochar) in this study in **Table 2**, it was concluded that the efficacy of our novel green synthesized nanocomposite was better than most of the nanomaterials synthesized in other studies.

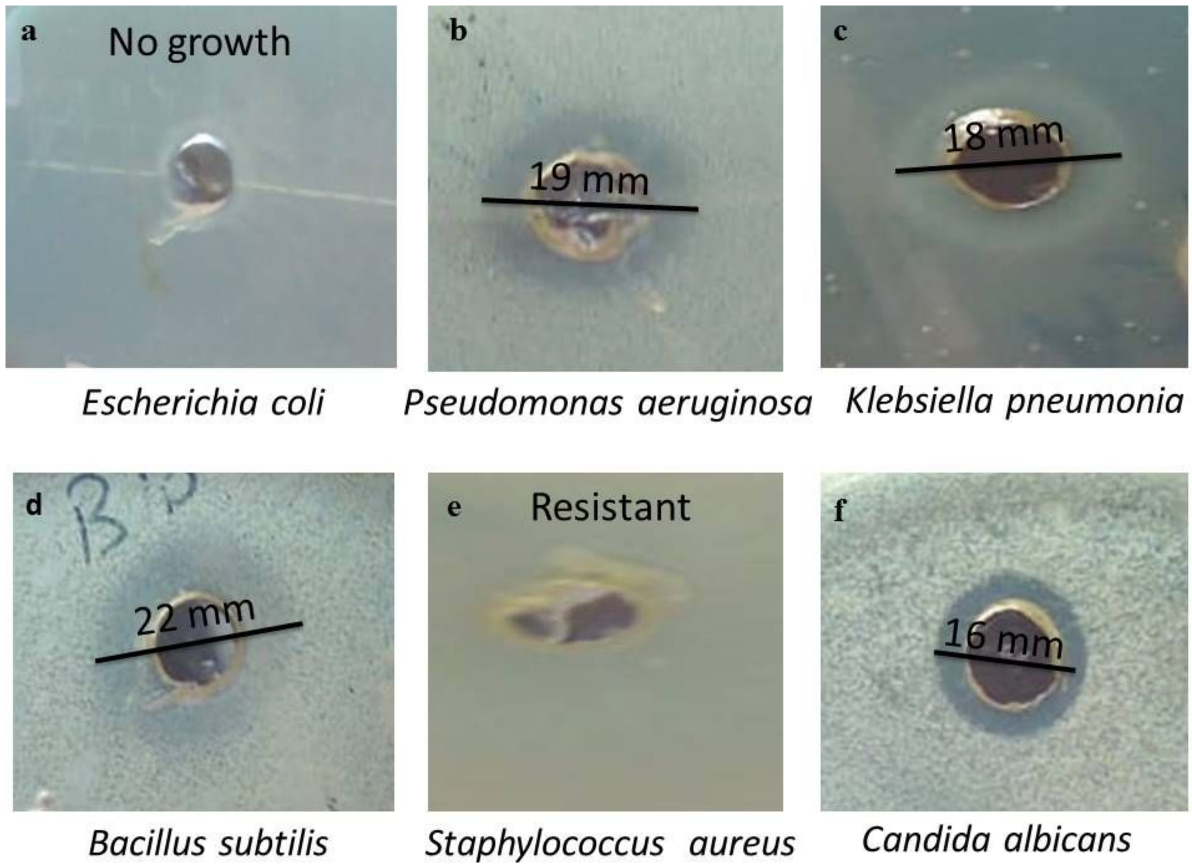

Fig. 5. Antimicrobial efficiency of Ag@biochar against **(a)** *Escherichia coli* **(b)** *Pseudomonas aeruginosa* **(c)** *Klebsiella pneumonia* **(d)** *Bacillus subtilis* **(e)** *Staphyllococus aureus* **(f)** *Candida albicans*.

Table 2. Comparison between the antimicrobial efficiency of Ag@biochar prepared in the current study and other AgNPs and AgNPs nanocomposite prepared in other studies.

Sample	Sample concentration ($mg.\ mL^{-1}$)	Bacterial strain	Zone of inhibition (mm)	Reference
Chitosan-silver nanoparticles (CS-AgNPs)	1	*Escherichia coli*	10	[36]
Methanol silver nanoparticles (SNPs)	100	*Staphylococcus aureus*	14.33	[37]
		Escherichia coli	10.33	
		Pseudomonas aeruginosa	13.67	

		Staphylococcus aureus	12.6	
		Staphylococcus aureus	13	
		Pseudomonas aeruginosa	16	
AgNPs embedded guar gum / gelatin nanocomposite	-	*Escherichia coli*	12.5	38
		Staphylococcus aureus	13	
		Pseudomonas aeruginosa	12.5	
Ag/GO nanocomposite	1	*Staphylococcus aureus*	15	39
		Escherichia coli	19	
copper-silver- titanium oxide nanocomposite (Cu-Ag-TiO_2)	0.5	*Staphylococcus aureus*	21	40
		Escherichia coli	16	
		Escherichia coli	16	
		Escherichia coli	9.3	
Ag@biochar	1	*Escherichia coli*	No growth (Sensitive)	This study
		Pseudomonas aeruginosa	19	
		Klebsiella pneumonia	18	
		Bacillus subtilis	22	
		Staphyllococus aureus	Resistant	
		Candida albicans	16	

Based on the current results, it was concluded that the greensynthesized Ag@biochar could be considered a broad spectrum and powerful disinfectant as it showed a well inhibitory effect against gram-negative, gram-positive bacteria, and also fungi. Therefore, Ag@biochar could be used as a promising antimicrobial agent in wastewater treatment.

3. Conclusions

Ag@biochar nanocomposite was synthesized using for the first time using *Chenopodium amperosidies*. AgNPs on biochar were mostly spherical with a size range of 25-35 nm. High removal efficiency of MB by Ag@biochar was demonstrated. Ag@biochar acquired a remarkable disinfection capability against *Escherichia coli*, *Pseudomonas aeruginosa*, *Klebsiella pneumonia*, *Bacillus subtilis*, and also *Candida albicans*. The synthesized Ag@biochar nanocomposite was proved to be an effective adsorbent and photocatalyst with a relatively low bandgap energy (1.9 eV). Thus, indicating that this novel nanocomposite could be an efficient candidate for the removal of toxic dyes from industrial wastewater as well as a disinfectant agent.

4. Materials and methods

4.1. Materials

Silver nitrate (99.9%, $AgNO_3$) and Methylene blue (MB) dye ($C_{16}H_{18}N_3SCl$, 319.85 g/mol) were purchased from Merck, USA.

4.2. Preparation of *Chenopodium amperosidies* extract

5 g of *C. amperosidies were* dissolved in 100 of deionized water, then the solution was subjected to heating and stirring at 80 °C, and finally it was filtered and the filtrate was preserved at 4 °C for further use.

4.3. Preparation of *Chenopodium amperosidies* -derived biochar

C. amperosidies is a medicinal plant found in countries with tropical, subtropical, temperate climate and some regions of the Mediterranean and Central America. It is a naturalized and common species in moist ground and canal banks in Egypt. *C. amperosidies* specimens were collected from their natural habitat on the northern coast of Egypt. The plant shoot was separated and then it was rinsed with deionized water several times in order to remove impurities or dirt. Then fragmented and allowed to dry in the open air followed by oven drying overnight at 60° C. Afterward dry stems were grinded in a stainless-steel mixer to obtain the fine powder. Afterward, 10 g of the dried powder were subjected to pyrolysis in a muffle furnace at 550 ºC for 3 h to obtain the biochar.

4.4. Green synthesis of Ag@biochar nanocomposite

0.79 g of biochar powder was dispersed in 100 mL of deionized water then 0.0158 g of $AgNO_3$ was added to the biochar dispersion and sonicated for 30 min. Afterward, 10 mL of *C. amperosidies* extract was added to the solution accompanied by stirring and heating at 80 °C for 1 h to reduce the silver ions on the surface of the biochar to form Ag@biochar nanocomposite. The formed Ag@biochar nanocomposite was separated via centrifugation, washed three times with deionized water and ethanol. Eventually, the Ag@biochar nanocomposite was dried in an oven at 60 °C for 24 h. The procedures are meticulously provided in **Scheme 1**.

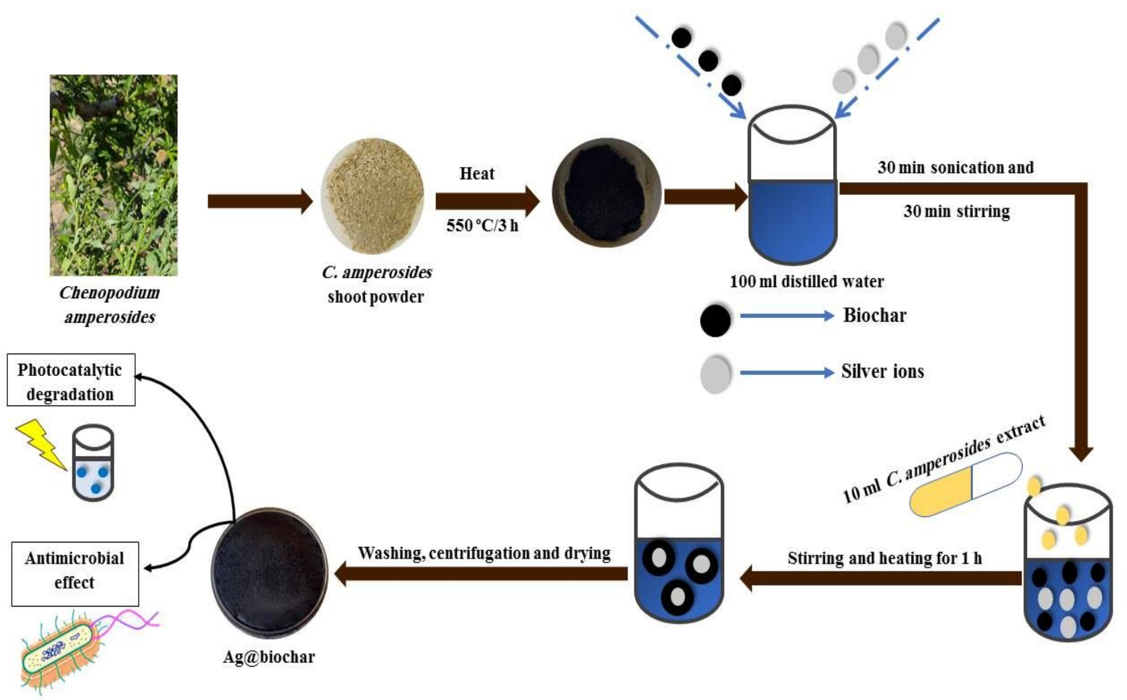

Scheme 1. Schematic representation for the preparation of the green Ag@biochar.

4.5. Characterization of Ag@biochar nanocomposite

The biogenic-reduction of the Ag^+ to AgNPs on the surface of biochar was confirmed via the UV–Visible spectroscopy measurements on a double-beam spectrophotometer (T70/T80 series UV/Vis Spectrophotometer, PG instruments Ltd, UK), in the scanning range 200 - 800 nm. The XRD measurements of Ag@biochar nanocomposite were done on an X-ray diffractometer (X'PERT PRO. Netherland) operated at a voltage of (45 kV) and current of (40 mA) with CuKa1 radiation ($\lambda = 1.54056$ A°) in the 2θ range from 20° to 80°. The morphological structure and elemental composition analysis were investigated via using scanning electron microscopy (SEM- JEOLJSM-IT 200, Japan) attached to an energy dispersive X-ray (EDX). X-ray Photoelectron Spectroscopy (XPS) was collected on K-ALPHA (Thermo Fisher Scientific, USA) with monochromatic X-ray Al K-alpha radiation -10 to 1350 eV spot size 400 micro m at pressure 10^{-9} mbar with full-spectrum pass energy 200 eV and narrow-spectrum 50 eV. Fourier Transform Infrared Spectroscopy (FT-IR) spectrum was conducted to assess the possible surface modification of biochar with AgNPs; the measurements were conducted for the grinded sample with KBr on a JASCO spectrometer over the range 4000 - 600 cm^{-1}. The specific surface area was estimated using Nitrogen adsorption/desorption isotherms (Micromeritics ASAP2020M analyzer, USA). Thermal stability was studied by TGA (Shimadzu–50, Japan). Zeta potentials of fabricated biochar and Ag@biochar nanocomposite were examined in a zeta potential analyzer (Zetasizer Nano ZS Malvern). Branueur–Emmet–Teller (BET) analysis was used to study surface area, the total pore volume, and pore diameter of the Ag@biochar nanocomposite using the nitrogen adsorption-desorption isotherm obtained using the multipoint BET and the Barette, Jovner & Halenda (BJH) process methods, respectively by a BET analyzer (Quantachrome NovaWin ©1994–2013, Quantachrome Instruments v11.03).

4.6. Photocatalytic experiments

Photocatalytic activity of the green synthesized Ag@biochar nanocomposite against (MB) dye was evaluated. 5 mg of Ag@biochar nanocomposite was added to 10 mL of three different concentrations of MB solution (10, 25, and 50 ppm). The Control experiment was carried out using 5 mg of biochar with an MB solution of a concentration of 25 ppm. Both test and control solutions were mixed for 30 min in dark conditions for adsorption/desorption equilibration. Then, the solutions were stirred under xenon lamp as a visible light source ($\lambda > 420$nm) and monitored. Next, 2 mL aliquots were removed and centrifuged at 17,000 rpm for 2 min to separate the solid nanocatalyst. The absorbance of the resultant supernatant of MB dye of both control and test solutions was measured at 664 nm wavelength in a quartz cuvette (path length 1 cm) using UV–vis spectroscopy (T70/T80 series UV/Vis Spectrophotometer, PG instruments Ltd, UK) scanning was done in the range 200-800 nm. Percentage of MB dye degradation was calculated by the following formula [41]:

$$\% \text{ Degradation} = \frac{A_o}{A} \times 100 \quad (1).$$

4.7. Antimicrobial test

Inoculum preparation: After overnight incubation, the tops of each of 3-5 colonies of pure culture of the organism to be tested (*Escherichia coli* (ATCC 8739), *Pseudomonas* *aeruginosa* (ATCC9027), *Klebsiella pneumonia* (ATCC 1388), *Bacillus subtilis* (ATCC 6633), *Staphyllococus aureus* (Mrsa) (ATCC 25923), and *Candida albicans* (ATCC 10231)) were touched with a loop and suspended in a sterile test tube containing 2mL saline. Turbidity of the suspended colonies was compared with the 0.5 McFarland turbidity standard equivalent to $2x10^8$ CFU/mL and the density of the organism suspension was adjusted by adding more bacteria or more sterile saline.

Preparation of seeded agar: Muller Hinton agar is weighed and dissolved in deionized water then sterilized by autoclaving after being divided into 25 mL portions into 6 separate flasks. Flasks left to cool to 50 °C then tested reference strains (1%) are added on sterile muller hinton agar. Flasks were shaken and poured onto sterile petri dishes and left to solidify. With a sterile cork borer, 3 wells (each 8 mm diameter) were made in each seeded agar plate.

Placing of tested materials (Ag@biochar): The panel of selected material to be evaluated was placed on the inoculated plates using a sterile automatic pipette directly onto its specific well after sterilization by filtration; the plates were put in the refrigerator overnight to allow diffusion of Ag@biochar material.

Incubation: Plates were incubated at 35±2°C for 24 h.

Reading results: All measurements were made with the unaided eye while viewing the back of the Petri dish a few inches above a non-reflecting background and illuminated with reflected light.

4.8. Statistical Analysis

All experiments were conducted in triplicate (n = 3), while the gained data were presented as a mean value corrected by the standard deviation (±SD).

Acknowledgement

This work was supported by SMARTWATIR, ERANETMED-3-227 project, Academy of Scientific Research and Technology.

AUTHOR INFORMATION

Abdelazeem S. Eltaweil - Department of Chemistry, Faculty of Science, Alexandria University, 163 Horria Avenue. El-Shatby, P.O. Box 832, Alexandria, Egypt.

abdelazeemeltaweil@alexu.edu.eg

Ahmed M. Abdelfatah - Green Technology Group, Environmental Sciences Department, Faculty of Science, Alexandria University, 21511, Alexandria, Egypt.

AhmedMohamedFatah@alexu.edu.eg

***Mohamed Hosny** - Green Technology Group, Environmental Sciences Department, Faculty of Science, Alexandria University, 21511, Alexandria, Egypt.

MohamedHosny@alexu.edu.eg / mohamedhosnymetal09@gmail.com

Manal Fawzy - Green Technology Group, Environmental Sciences Department, Faculty of Science, Alexandria University, 21511, Alexandria, Egypt.

National Egyptian Biotechnology Experts Network, National Egyptian Academy for Scientific Research and Technology.

dm_fawzy@yahoo.com / manal.fawzy@alexu.edu.eg

Authors' contribution: Abdelazeem S. Eltaweil suggested the idea of this article and was responsible for conceptualization, supervision, validation and reviewing the final manuscript. Ahmed M. Abdelfatah was responsible for conducting the laboratory experiments and writing the original draft. Mohamed Hosny was responsible for the investigation, formal analysis, methodology, data curation, visualization and writing the original draft. Manal Fawzy was responsible for conceptualization, funding acquisition, project administration, supervision, validation and reviewing the final manuscript.

Conflict of interests: There are no conflicts of interest.

References

1. Razavi-Khosroshahi, H.; Wenhao, S.; Fuji, M., Synthesis of TiO2 hollow nanoparticles with different shell thickness and effect of structure on photocatalytic activity. *Solid State Sciences* **2020,** *103*, 106179.

2. Hidalgo-Jimenez, J.; Wang, Q.; Edalati, K.; Cubero-Sesín, J. M.; Razavi-Khosroshahi, H.; Ikoma, Y.; Gutiérrez-Fallas, D.; Dittel-Meza, F. A.; Rodríguez-Rufino, J. C.; Fuji, M., Phase transformations, vacancy formation and variations of optical and photocatalytic properties in TiO2-ZnO composites by high-pressure torsion. *International Journal of Plasticity* **2020,** *124*, 170-185.

3. Abdelfatah, A. M.; Fawzy, M.; Elkhouly, M.; Eltaweil, A. S., Efficient Adsorptive Removal of Tetracycline from Aqueous Solution using Phytosynthesized Nano-zero Valent Iron. *Journal of Saudi Chemical Society* **2021**, 101365.

4. Li, Y.; Wang, H.; Xie, J.; Hou, J.; Song, X.; Dionysiou, D. D., Bi2WO6-TiO2/starch composite films with Ag nanoparticle irradiated by γ-ray used for the visible light photocatalytic degradation of ethylene. *Chemical Engineering Journal* **2021,** *421*, 129986.

5. Hosny, M.; Fawzy, M.; Abdelfatah, A. M.; Fawzy, E. E.; Eltaweil, A. S., Comparative study on the potentialities of two halophytic species in the green synthesis of gold nanoparticles and their anticancer, antioxidant and catalytic efficiencies. *Advanced Powder Technology* **2021**.

6. Abdelfatah, A. M.; Fawzy, M.; Eltaweil, A. S.; El-Khouly, M. E., Green Synthesis of Nano-Zero-Valent Iron Using Ricinus Communis Seeds Extract: Characterization and Application in the Treatment of Methylene Blue-Polluted Water. *ACS Omega* **2021**.

7. Eltaweil, A. S.; Elshishini, H. M.; Ghatass, Z. F.; Elsubruiti, G. M., Ultra-high adsorption capacity and selective removal of Congo red over aminated graphene oxide modified Mn-doped UiO-66 MOF. *Powder Technology* **2021,** *379*, 407-416.

8. El-Borady, O. M.; Fawzy, M.; Hosny, M., Antioxidant, anticancer and enhanced photocatalytic potentials of gold nanoparticles biosynthesized by common reed leaf extract. *Applied Nanoscience* **2021**, 1-12.

9. Hosny, M.; Fawzy, M., Instantaneous phytosynthesis of gold nanoparticles via Persicaria salicifolia leaf extract, and their medical applications. *Advanced Powder Technology* **2021,** *32* (8), 2891-2904.

10. LewisOscar, F.; Nithya, C.; Vismaya, S.; Arunkumar, M.; Pugazhendhi, A.; Nguyen-Tri, P.; Alharbi, S. A.; Alharbi, N. S.; Thajuddin, N., In vitro analysis of green fabricated silver nanoparticles (AgNPs) against Pseudomonas aeruginosa PA14 biofilm formation, their application on urinary catheter. *Progress in Organic Coatings* **2021,** *151*, 106058.

11. Fazal, T.; Razzaq, A.; Javed, F.; Hafeez, A.; Rashid, N.; Amjad, U. S.; Rehman, M. S. U.; Faisal, A.; Rehman, F., Integrating adsorption and photocatalysis: A cost effective strategy for textile wastewater treatment using hybrid biochar-TiO2 composite. *Journal of hazardous materials* **2020,** *390*, 121623.

12. Mian, M. M.; Liu, G., Recent progress in biochar-supported photocatalysts: synthesis, role of biochar, and applications. *RSC advances* **2018,** *8* (26), 14237-14248.

13. Wang, T.; Liu, S.; Mao, W.; Bai, Y.; Chiang, K.; Shah, K.; Paz-Ferreiro, J., Novel Bi2WO6 loaded N-biochar composites with enhanced photocatalytic degradation of rhodamine B and Cr (VI). *Journal of hazardous materials* **2020,** *389*, 121827.

14. Dai, W.; Xu, M.; Zhao, Z.; Zheng, J.; Huang, F.; Wang, H.; Liu, C.; Xiao, R., Characteristics and quantification of mechanisms of Cd2+ adsorption by biochars derived from three different plant-based biomass. *Arabian Journal of Chemistry* **2021,** *14* (5), 103119.

15. Rajkumar, R.; Ezhumalai, G.; Gnanadesigan, M., A green approach for the synthesis of silver nanoparticles by Chlorella vulgaris and its application in photocatalytic dye degradation activity. *Environmental Technology & Innovation* **2021,** *21*, 101282.

16. Hashim, N.; Paramasivam, M.; Tan, J. S.; Kernain, D.; Hussin, M. H.; Brosse, N.; Gambier, F.; Raja, P. B., Green mode synthesis of silver nanoparticles using Vitis vinifera's tannin and screening its antimicrobial activity/apoptotic potential versus cancer cells. *Materials Today Communications* **2020,** *25*, 101511.

17. Dai, Z.; Meng, J.; Muhammad, N.; Liu, X.; Wang, H.; He, Y.; Brookes, P. C.; Xu, J., The potential feasibility for soil improvement, based on the properties of biochars

pyrolyzed from different feedstocks. *Journal of soils and sediments* **2013,** *13* (6), 989-1000.

18. Adeniyi, A. G.; Ighalo, J. O.; Onifade, D. V., Biochar from the thermochemical conversion of orange (Citrus sinensis) peel and Albedo: product quality and potential applications. *Chemistry Africa* **2020,** *3* (2), 439-448.

19. Ma, Z.; Liu, J.; Liu, Y.; Zheng, X.; Tang, K., Green synthesis of silver nanoparticles using soluble soybean polysaccharide and their application in antibacterial coatings. *International Journal of Biological Macromolecules* **2021,** *166*, 567-577.

20. Fleutot, S.; Martinez, H.; Dupin, J.-C.; Baraille, I.; Forano, C.; Renaudin, G.; Gonbeau, D., Experimental (X-Ray Photoelectron Spectroscopy) and theoretical studies of benzene based organics intercalated into layered double hydroxide. *Solid state sciences* **2011,** *13* (9), 1676-1686.

21. Zotti, G.; Zecchin, S.; Schiavon, G.; Louwet, F.; Groenendaal, L.; Crispin, X.; Osikowicz, W.; Salaneck, W.; Fahlman, M., Electrochemical and XPS studies toward the role of monomeric and polymeric sulfonate counterions in the synthesis, composition, and properties of poly (3, 4-ethylenedioxythiophene). *Macromolecules* **2003,** *36* (9), 3337-3344.

22. Xi, Y.; Sun, Z.; Hreid, T.; Ayoko, G. A.; Frost, R. L., Bisphenol A degradation enhanced by air bubbles via advanced oxidation using in situ generated ferrous ions from nano zero-valent iron/palygorskite composite materials. *Chemical Engineering Journal* **2014,** *247*, 66-74.

23. Liu, Y.; Yang, S.; Yin, S.-N.; Feng, L.; Zang, Y.; Xue, H., In situ construction of fibrous AgNPs/g-C3N4 aerogel toward light-driven COx-free methanol dehydrogenation at room temperature. *Chemical Engineering Journal* **2018,** *334*, 2401-2407.

24. Ghodake, G.; Kim, M.; Sung, J.-S.; Shinde, S.; Yang, J.; Hwang, K.; Kim, D.-Y., Extracellular synthesis and characterization of silver nanoparticles—Antibacterial activity against multidrug-resistant bacterial strains. *Nanomaterials* **2020,** *10* (2), 360.

25. Hosny, M.; Fawzy, M.; El-Borady, O. M.; Mahmoud, A. E. D., Comparative study between Phragmites australis root and rhizome extracts for mediating gold nanoparticles synthesis and their medical and environmental applications. *Advanced Powder Technology* **2021**.

26. Hamouda, R. A.; Abd El-Mongy, M.; Eid, K. F., Comparative study between two red algae for biosynthesis silver nanoparticles capping by SDS: Insights of characterization and antibacterial activity. *Microbial pathogenesis* **2019,** *129*, 224-232.

27. Eltaweil, A.; Mohamed, H. A.; Abd El-Monaem, E. M.; El-Subruiti, G., Mesoporous magnetic biochar composite for enhanced adsorption of malachite green dye: Characterization, adsorption kinetics, thermodynamics and isotherms. *Advanced Powder Technology* **2020,** *31* (3), 1253-1263.

28. Mansaray, K.; Ghaly, A., Thermal degradation of rice husks in nitrogen atmosphere. *Bioresource technology* **1998,** *65* (1-2), 13-20.

29. Huang, D.; Luo, H.; Zhang, C.; Zeng, G.; Lai, C.; Cheng, M.; Wang, R.; Deng, R.; Xue, W.; Gong, X., Nonnegligible role of biomass types and its compositions on the formation of persistent free radicals in biochar: insight into the influences on Fenton-like process. *Chemical Engineering Journal* **2019,** *361*, 353-363.

30. Singh, J.; Dhaliwal, A. S., Plasmon-induced photocatalytic degradation of methylene blue dye using biosynthesized silver nanoparticles as photocatalyst. *Environ Technol* **2020,** *41* (12), 1520-1534.

31. Fairuzi, A. A.; Bonnia, N. N.; Akhir, R. M.; Abrani, M. A.; Akil, H. M., Degradation of methylene blue using silver nanoparticles synthesized fromimperata cylindricaaqueous extract. *IOP Conference Series: Earth and Environmental Science* **2018,** *105*, 012018.

32. Abdel Messih, M. F.; Ahmed, M. A.; Soltan, A.; Anis, S. S., Synthesis and characterization of novel Ag/ZnO nanoparticles for photocatalytic degradation of methylene blue under UV and solar irradiation. *Journal of Physics and Chemistry of Solids* **2019,** *135*, 109086.

33. Panchal, P.; Paul, D. R.; Sharma, A.; Choudhary, P.; Meena, P.; Nehra, S., Biogenic mediated Ag/ZnO nanocomposites for photocatalytic and antibacterial activities towards disinfection of water. *Journal of colloid and interface science* **2020,** *563*, 370-380.

34. Moser, D.; Biere, K.; Han, B.; Hoerl, M.; Schelling, G.; Choukér, A.; Woehrle, T., COVID-19 Impairs Immune Response to Candida albicans. *Frontiers in immunology* **2021,** *12*.

35. Varghese, R.; Almalki, M. A.; Ilavenil, S.; Rebecca, J.; Choi, K. C., Silver nanopaticles synthesized using the seed extract of Trigonella foenum-graecum L. and their antimicrobial mechanism and anticancer properties. *Saudi journal of biological sciences* **2019,** *26* (1), 148-154.

36. Tharani, S.; Bharathi, D.; Ranjithkumar, R., Extracellular green synthesis of chitosan-silver nanoparticles using Lactobacillus reuteri for antibacterial applications. *Biocatalysis and Agricultural Biotechnology* **2020,** *30*, 101838.

37. Yousaf, H.; Mehmood, A.; Ahmad, K. S.; Raffi, M., Green synthesis of silver nanoparticles and their applications as an alternative antibacterial and antioxidant agents. *Materials Science and Engineering: C* **2020,** *112*, 110901.

38. Khan, N.; Kumar, D.; Kumar, P., Silver nanoparticles embedded guar gum/gelatin nanocomposite: Green synthesis, characterization and antibacterial activity. *Colloid and Interface Science Communications* **2020,** *35*, 100242.

39. Jeronsia, J. E.; Ragu, R.; Sowmya, R.; Mary, A. J.; Das, S. J., Comparative investigation on Camellia Sinensis mediated green synthesis of Ag and Ag/GO nanocomposites for its anticancer and antibacterial efficacy. *Surfaces and Interfaces* **2020,** *21*, 100787.

40. Ghosh, M.; Mandal, S.; Roy, A.; Paladhi, A.; Mondal, P.; Hira, S. K.; Mukhopadhyay, S. K.; Pradhan, S. K., Synthesis and characterization of a novel drug conjugated copper-silver-titanium oxide nanocomposite with enhanced antibacterial activity. *Journal of Drug Delivery Science and Technology* **2021,** *62*, 102384.

41. Eltaweil, A. S.; Fawzy, M.; Hosny, M.; Abd El-Monaem, E. M.; Tamer, T. M.; Omer, A. M., Green synthesis of platinum nanoparticles using Atriplex halimus leaves for potential antimicrobial, antioxidant, and catalytic applications. *Arabian Journal of Chemistry* **2021**, 103517.

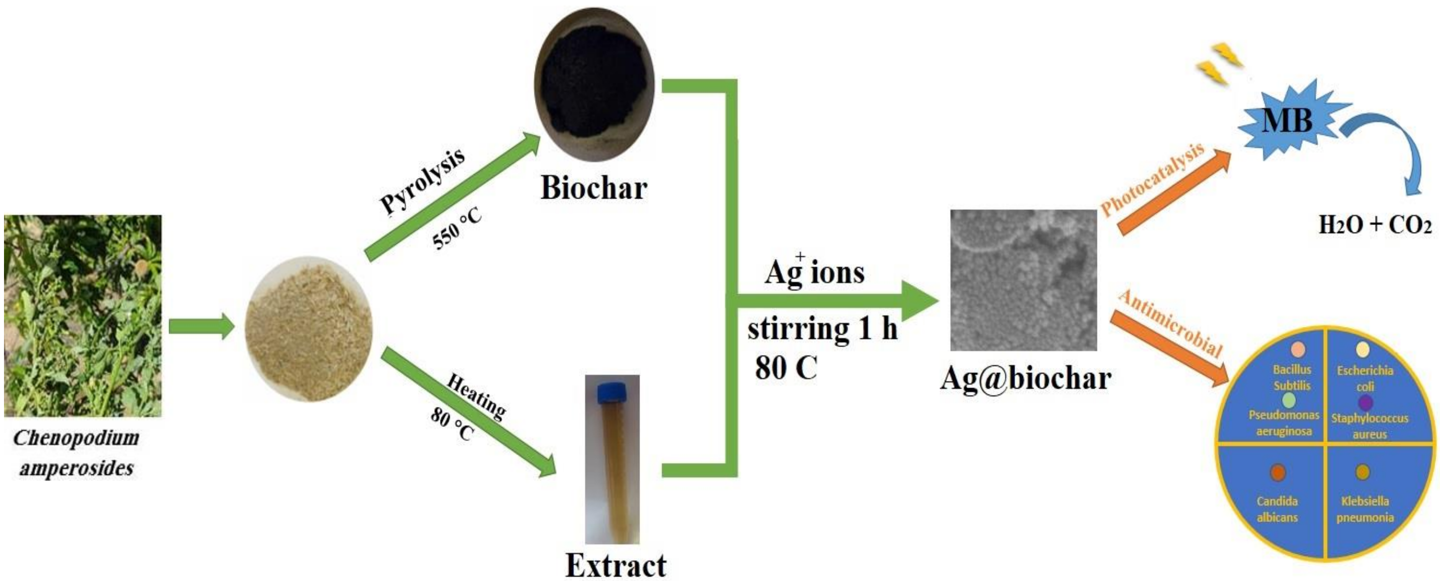
Chenopodium amperosides
Pyrolysis
550 °C
Biochar
Heating
80 °C
Extract
Ag+ ions
stirring 1 h
80 C
Ag@biochar
Photocatalysis
MB
H2O + CO2
Antimicrobial
Bacillus Subtilis
Escherichia coli
Pseudomonas aeruginosa
Staphylococcus aureus
Candida albicans
Klebsiella pneumonia